Organic Matter Oxidation of the Tégulines Clay formation, (Paris Basin, France): Spatial Heterogeneities

Mathieu Le Meur, Mohammed Boussafir, Claude Le Milbeau, Mathieu Debure, Francis Claret, Jean-Charles Robinet, Catherine Lerouge

Journal Pre-proof

Organic Matter Oxidation of the Tégulines Clay formation, (Paris Basin, France): Spatial Heterogeneities

Le Meur Mathieu, Boussafir Mohammed, Le Milbeau Claude, Debure Mathieu, Claret Francis, Robinet Jean-Charles, Lerouge Catherine

Please cite this article as: Mathieu, L.M., Mohammed, B., Claude, L.M., Mathieu, D., Francis, C., Jean-Charles, R., Catherine, L., Organic Matter Oxidation of the Tégulines Clay formation, (Paris Basin, France): Spatial Heterogeneities, *Applied Geochemistry*, https://doi.org/10.1016/j.apgeochem.2021.105093.

This is a PDF file of an article that has undergone enhancements after acceptance, such as the addition of a cover page and metadata, and formatting for readability, but it is not yet the definitive version of record. This version will undergo additional copyediting, typesetting and review before it is published in its final form, but we are providing this version to give early visibility of the article. Please note that, during the production process, errors may be discovered which could affect the content, and all legal disclaimers that apply to the journal pertain.

Organic Matter Oxidation of the Tégulines Clay formation, (Paris Basin, France): Spatial Heterogeneities

Le Meur Mathieu[a,b], Boussafir Mohammed[a,e], Le Milbeau Claude[a], Debure Mathieu[c], Claret Francis[c], Robinet Jean-Charles[d] & Lerouge Catherine[c]

(a)

(a) Université d'Orléans, CNRS, BRGM, ISTO, UMR 7327, F-45071, Orléans, France

(b) EA 4592 G&E, Bordeaux INP - Université Bordeaux Montaigne - Carnot ISIFoR, 1 allée F. Daguin, 33607 Pessac, France

(c) BRGM, BP36009, 45060 OrléansCedex 2, France

(d) ANDRA 1-7 rue Jean Monnet 92298 Chatenay Malabry, France

(e) Université François Rabelais de Tours, EA 6293 GéHCO, Tours, France

Corresponding authors: m.lemeur@hotmail.fr; mathieu.le_meur@bordeaux-inp.fr

Abstract

Samples of Albian Tégulines Clay outcropping near Brienne-le-Château in the eastern part of the Paris Basin were subjected to a geochemical characterization of organic matter (OM), combining OM bulk Rock-Eval analysis (RE), organic petrography and molecular analysis. In this study, the objective was to investigate the oxidation of natural organic matter in critical zone developed in early reduced marine clay formation. For that purpose, core samples from three boreholes crosscutting the Tégulines Clay formation down to the Greensands were selected. Several meters of Brienne marls preserved Tégulines Clay from atmosphere and therefore from high weathering and high oxidation in AUB240 borehole, whereas Tégulines Clay were weathered in their upper part in AUB1010 and in AUB230 boreholes as a result to their vicinity to the surface. The results showed that the Total Organic Carbon (TOC) contents in all clays are very low, ranging between 0.3 and 0.7 wt.%. The RE bulk data and Tmax parameter of OM in preserved Tégulines Clay indicate that the OM is immature. The organic petrography shows a predominance of gel-like amorphous OM preserved by natural sulphurisation in anoxic environments. Organic matter in Tégulines Clay from the AUB230 and AUB1010 boreholes show similar characteristics. The OM at the top of Tégulines Clay contains large amounts of oxidized lignocellulosic debris and has high RE Oxygen-Index values. In the first upper 10 m of the clays, the RE bulk, organic petrography and molecular data revealed oxidative events (high OI and high oxidized debris contents). Below 10 m, the OM is almost preserved. The OM in the reduced marine Tégulines Clay formation is very little functionalized and seems to be slightly reactive but not negligibly with the inorganic fractions in presence of oxygen.

Keywords: Tégulines Clay formation, weathering profile, oxidation, Bulk organic characterization, Palynofacies, Molecular organic characterization

1 Introduction

40

41 Clay-rich geological formations are considered by many countries as natural barriers for radioactive

42 waste isolation due to their low permeability and their sorption properties preventing the release of

43 radioactive substances towards the biosphere. Most of previous investigations concerning clay-rich

44 formations focus on deep systems (> 100 m) without direct interface with biosphere-atmosphere

45 (Hendry and Wassenaar 2000; Hautevelle et al., 2007; Altmann et al. 2012). In the context of sub-surface

46 waste repository, the vicinity of the surface can affect the solid-fluid equilibrium system of the

47 geological formation due to weathering and oxidation phenomena involving in turn potential effects on

48 solute transport properties with depth. Such phenomena in clay-rich formations are scarce and have been

49 recently evidenced in the Lower Cretaceous Tégulines marine-clay formation (Tégulines Clay) near

50 Brienne-Le-Chateau (Aube department, France) investigated for a decade in the context of sub-surface

51 repository for low-level radioactive waste (Debure et al., 2020; Debure et al., 2018; Duffy et al., 2014;

52 Lerouge et al., 2018, 2020). Like most of the marine clay-rich formations, Tégulines Clay evolved under

53 reduced geochemical conditions during early diagenesis and its burial (Lerouge et al. 2018). In the

54 studied area, weathering and oxidation phenomena including changes of mineralogy, chemistry, and

55 petrophysical properties occur in Tégulines Clay at vicinity of the surface, due to interactions with

56 oxygen and meteoric waters. A gradual oxidation profile developed in the clay formation and the

57 resulting effects on pore water chemistry were evidenced based on several indicators as sulfur and iron

58 oxidation states (Lerouge et al., 2018) and the changes of CO_2 partial pressure (Lerouge et al., 2020).

59 Reactivity of Organic Matter (OM) with oxygen is suspected to play a role on CO_2 and redox regulation

60 of the Tégulines Clay at vicinity of the surface.

61 In this study, we propose to investigate the reactivity of natural OM in Tégulines Clay as a marker of

62 weathering and oxidation, using bulk and molecular techniques in the objective to better evaluate how

63 atmosphere interacts with the rock and regulates its solid-fluid systems with depth. Organic Matter (OM)

64 bulk analysis is firstly achieved by Rock-Eval analyses associated with palynofacies. This analytical

65 approach allows determining the OM composition and its quality in term of maturity, refractory and

66 redox state. Additional molecular organic geochemistry secondly completes the OM characterization,

67 in term of origins (marine/terrestrial), maturity (saturated hydrocarbons) and oxidation (deposition mode

68 and weathering). Such type of approach was previously applied in deep clay-rich geological formation

69 (Deniau et al., 2008; Elie et al. 2000; Elie and Mazurek, 2008; Hautevelle et al. 2007; Landais et al.

70 1991; Landais and Elie, 1999) and is here challenged in a sub-surface context.

2 Materials and methods

71

2.1 Geological setting and mineralogy

72

73

74 The studied area is located near Brienne-le-Chateau in the eastern part of the Paris Basin (Aube

75 department, Figure 1 (a,b)). The Gault clay formation (Gault Clay) consists of siliciclastic shales

76 deposited in an open marine environment from Middle to Upper Albian (Lower Cretaceous) on the

77 Greensands formation (Amedro et al., 2014). The stratotype of the Gault Clay defined in the Aube

78 department consists of Tégulines Clay (82 m) overlaid by the Brienne marls (43 m). At the maximum

79 burial of the Paris Basin, temperatures reached 30-36°C in the Gault Clay (Lerouge et al., 2018). In

80 Early Miocene, the Paris Basin chalk formations were eroded. Nowadays the Gault Clay outcrops as an

81 8-10 km wide and 80-km long band of terranes-oriented NE-SW through the Aube department. The

82 Brienne marls only subsist in the western part of the studied area, elsewhere the Tégulines Clay outcrops.

83 Its thickness increases from east to west between 60 and 120 m. Locally few meters of Quaternary

84 surficial formations overly Gault Clay.

85 The unweathered Tégulines Clay essentially consists of clay minerals (47-72 %) associated with quartz-

86 feldspar (28-43 %), carbonates (0-22%), and minor pyrite and phosphate nodules. Mineral variability in

87 unweathered Tégulines Clay is mainly vertical (Fig. 1 (c)). The first 9-12 meters at the bottom of the

88 clay formation is characterized as a clay-quartz rich unit (named UAQ), with the highest quartz –

89 feldspar silty content (46 %) and the lowest carbonate content (3.5 %). The next 35-40 m constitutes a

90 clay-rich unit (named UA) with a clay average content of 51 %, and intermediate carbonate and quartz-

91 feldspar silty contents. The last 20-25 meters at the top of the clay formation constitutes a carbonate-

92 clay rich unit (named UAC), characterized by the highest carbonate content (9-25 %) and the lowest

93 quartz – feldspar silty content (30 %). The UAC unit constitutes a transitory term with the Brienne marls

94 (Lerouge et al. 2018).

95

96   2.2 Materials, sampling campaigns

97   Fifty-three core samples of Tégulines Clay were selected among three boreholes for the study of organic

98   matter: 7 from the AUB240 borehole (2018 drilling campaign), 31 from the AUB230 borehole (2017

99   drilling campaign) and 15 from the AUB1010 borehole (2015 drilling campaign). Additional samples

100   of soil and Quaternary surficial formations were collected in a trench (TPH 1-1) corresponding to the

101   first meters of the AUB230 borehole, due to the difficulty to recover the first meters during the drilling.

102   In the AUB240 borehole, surficial formations and ~12 meters of Brienne marls overlaid the Tégulines

103   Clay, allowing a protection for the Tégulines Clay. Consequently, core samples collected in the

104   Tégulines horizon from this borehole can be considered as the most representative of compacted pristine

105   Tégulines Clay. The AUB230 borehole, located on a ridge top in cropland, crosscut ~ 30 cm of brown

106   soil, ~ 5 m of surficial formations (sandy loam) and ~ 63 m of Tégulines Clay down to Greensands. The

107   AUB1010, located down the valley, crosscut less than 2 m of surficial formations and ~ 33 m of

108   Tégulines Clay down to Greensands (Fig. 3).

109   Major mineralogy of the Tégulines Clay core samples from the AUB230 and AUB1010 deduced from

110   XRD data treatment are consistent (Lerouge et al., 2018, 2020) (fig. 1 (c)).

111   At the top of Tégulines Clay from the AUB230 and AUB1010 boreholes, claystone is sticky and grey

112   with iron oxi-hydroxides. Interactions between Tégulines Clay and surficial oxidizing waters induce

113   mineralogical changes such as pyrite oxidation, calcite dissolution and precipitation of iron hydroxides

114   and gypsum between the top of the formation down to ~11 m. Detailed mineralogical, geochemical and

115   petrophysical work on Tégulines Clay of the AUB1010 and AUB230 boreholes rather indicated an

116   extension of the oxidation front down to ~20 m depth (Lerouge et al., 2018, 2020). Current investigations

117   provide evidence of ancient root network development down to ~12 m depth at least.

118

119   2.3 Methodology
120   2.3.1 Rock-Eval analysis (RE)

121   The type, quality and amount of OM preserved in TCF samples before and after thermal maturation

122   were determined using new Rock-Eval 6® pyrolysis (Vinci Technologies, Rueil Malmaison). About 50

123   to 60 mg of powdered and dried samples were used for the analysis depending on the estimated OM

124 contents. The pyrolysis program involved an isothermal stage at 200 °C, held 2 min under inert gas

125 (helium); the temperature was then raised to 650 °C (30 °C.min-1) and held for 3 min. The oxidation

126 phase started with an isothermal stage at 400 °C under purified air. Then, the oven temperature was

127 raised to 750 °C (at 30 °C.min−1) and held for 5 min. New Rock-Eval 6® classical parameters and their

128 significance were explained by Espitalie et al. (1985a,b) and Lafargue et al. (1998). 4 parameters were

129 used in the present study: (i) the total organic carbon content (TOC, wt %), which accounts for the

130 quantity of OM calculated from the integration of the amount of thermo-evaporated free hydrocarbons

131 (S1 peak), hydrocarbons produced by kerogen pyrolysis (S2), S3CO and S3CO2 produced by the

132 breakdown of kerogen under inert gas and S4CO and S4CO2 produced by the oxidation and the

133 pyrolysis of residual carbon under purified air; (ii) the oxygen index (OI, mg CO_2.g−1 TOC), which is

134 the oxygenated quality of OM calculated from the S3 peak; (iii) the hydrogen index (HI, mg HC.g−1

135 TOC), which represents the amount of HC quality produced during pyrolysis (calculated from the S2

136 peak); (iv) the Tmax, which is deduced from the Tpic of Rock-Eval VI. Tpic is the temperature of the

137 peak oil production during pyrolysis. Tmax is often used as an OM maturity indicator (Espitalie et al.,

138 1985a,b). The Total Organic Carbon (TOC), the Hydrogen Index (HI) and the Oxygen Index (OI) are

139 the 3 main parameters used in environmental science (Di-Giovanni et al. 1998, Boussafir et al. 2012).

140 T_{peak} deduced from S2 spectra is also used in environmental science. It is the temperature of the oven

141 for the maximum hydrocarbon released.

142 Thanks to the deconvolution of the S2 pyrolysis spectra using Peakfit software (SPSS®), we were able

143 to show the presence of 5 elemental Gaussian distributions describing the release of the different

144 pyrolytic molecular families at T_{peak} temperatures (+- 20°C) of 260 °C, 310 °C, 370 °C, 460 °C and 560

145 °C. The relative contribution of these different pyrolytic molecular compounds to the signal was also

146 semi-quantified by the calculation of peak surfaces of the corresponding Gaussians plotted to those of

147 the entire S2 signal surface.

148 2.3.2 Microscopic investigations

149 Initially developed by Combaz (1964), the quantitative organic petrography is a method that consists to

150 study thin slides under a microscope that permit the identification and the quantification of the organic

151   compounds present in a constant amount of sediments (1 cm^3 or 1 gram) after the elimination of

152   carbonate and silicate by hydrochloric and hydrofluoric treatments (Graz et al. 2010). Optical

153   investigations were performed with a DMR XP Leica microscope by using the transmitted light mode.

154   The approach is based on the distinction of different categories of petrographic components

155   characterized by their optical, form properties and, origins (Combaz 1980; Tyson 1995). This

156   quantification was carried out on a minimum of 500 particles with a 50x magnification objective (Di-

157   Giovanni et al. 1998, Sebag et al. 2006 a,b, Graz et al. 2010). To achieve absolute quantification of

158   palynofacies, a pollen standard of precise concentration has been introduced in the samples. (Battarbee

159   and Kneen 1982; Vernal et al. 1987) In this study, the standard chosen is *Cupressus sp.* Because of its

160   strong reaction under UV excitation thus eliminating any confusion. Three main classes were

161   distinguished in the different samples: the amorphous organic matter, without any biological apparent

162   structures, lignocellulosic debris inherited from higher plant and other particles distinguished by their

163   easily recognizable morphology. Different categories were observed in these three main classes and are

164   detailed in Table 1 and Figure 2.

165   2.3.3 Lipid molecular analysis

166   Lipids were extracted from ca. 5 g of dried sediment using a Dionex ASE 200 with a dichloromethane

167   (DCM): methanol (MeOH) mixture (9:1 v/v; at 100 °C and 1000 psi for 5 min in 3 cycles). After solvent

168   evaporation, the total extract was then separated into neutral, acid and polar fractions using liquid

169   chromatography with aminopropyl bonded silica as solid phase (Jacob et al., 2005). 5α(H)-cholestane

170   was added as an internal standard to the neutral and acid fractions and dried under N2 flux. The acid

171   fraction samples were then methylated by adding a mixture of anhydrous MeOH and acetyl chloride

172   kept at 60 °C for 1 h. The obtained methyl ester and neutral fractions were then derivatized by reacting

173   40 µl *N,O*-bis(trimethylsilyl)trifluoroacetamide (BSTFA) in 60 µl pyridine at 60 °C for 1 h. and analyzed

174   by GC-MS.

175   GC-MS analyses were performed on a Trace GC coupled to a TSQ Quantum XLS mass spectrometer

176   (both from Thermo Scientific). Gas chromatograph (GC) was fitted with a Trace Gold TG-5MS capillary

177   column (60 m x 0.25 mm id, 0.25 µm film thickness). The sample was dissolved in toluene and injected

178   with a splitless mode in a 2 µl volume. The injector temperature set at 280 °C. Helium was the carrier

179   gas at a flow rate of 1 ml.min^{-1}. The GC operating conditions were as follows: temperature increase from

180   40 to 120 °C at 30 °C/ min and 120 to 310 °C at 3 °C/min with a final isothermal hold at 310 °C for 68

181   min. The mass spectrometer was operated in the electron ionization (EI) mode at 70 eV and scanned

182   from 50 to 650 Daltons. The identifications of the different peaks were based on a comparison of mass

183   spectra with published data. Lipids concentration was estimated by the comparison of TIC area of each

184   lipid with that of the internal standard and normalized to the weight of the extracted sample.

185

186   3. Results and discussion

187   3.1 Rock Eval data

188   3.1.1 Quantitative and qualitative characterization of the OM

189   For all the analyzed samples, the results obtained by Rock-Eval analysis are presented in Figure 3 and

190   Supplementary data 1. While, the TOC values indicates an organic content below 1 wt.% for the

191   Tégulines Clay, the content is varying with the depth with an increase from 0.36 to 0.59 wt.% in the first

192   10 meters and with a small variation around a 0.53 mean value in the deeper part. The Hydrogen Index

193   (HI) and the Oxygen Index (OI) were reported both in the Figure 3 as a function of depth and in a Pseudo

194   van Krevelen diagram to characterize the OM type (Fig. 4). Again, as detailed hereafter the first 10 m

195   show a different behavior with a decrease of HI and OI while below 10 m OI and HI are homogeneous

196   and showed almost no variation with depth

Soil and Quaternary formation

198   Soil and Quaternary formation are available only for AUB230. The soil at the top of the AUB230

199   borehole (TPH1-1 0-30 cm) has a TOC of 1.45 wt.%, and is characterized by high HI and OI values,

200   revealing oxygenated immature OM. These data are in good agreement with soil data of the literature

201   (Copard et al. 2006).

202   Quaternary surficial formation at the top of the Tégulines Clay in the AUB230 borehole does not contain

203   any analyzable OM, except the samples at 4 and 5 m, that corresponds to the transition with Tégulines

204 Clay. The latter show low but valid TOC, and a hydrogenated quality (HI) and oxygenated (OI) average

205 ranging respectively between 100 and 286 mg HC. g^{-1} TOC and 268 and 307 mg CO2. g^{-1} TOC.

206 *Tégulines Clay*

207 Tégulines Clay in the AUB240 borehole (Fig. 3) shows homogenous RE parameters (TOC, HI, OI)

208 suggesting stable OM and can be considered as a reference in term of types and preservation of OM in

209 the clay formation for this study. TOC values are extremely low, ranging between 0.4 and 0.7 wt.%. The

210 HI through the clay formation varies between 17 mg HC. g^{-1} TOC and 30 mg HC. g^{-1} TOC. The OI is

211 ranging between 122 and 176 mg $CO_2.g^{-1}$ TOC.

212 TOC values of Tégulines Clay in the AUB230 borehole (AUB230 6.10 - 68.45 m) range between 0.4 –

213 and 0.7 % and are almost similar to that of Tégulines Clay in borehole AUB240. At the top of the clay

214 formation at 6.00-6.10 m, TOC value of 0.4 is low compared to the soil (TPH1-1 0-30) and remains

215 almost homogeneous until 45 m. In the deepest part (>45 m), the TOC increases slightly to reach 0.8

216 wt. %. At 70 m toward the transition with Greensands, the TOC decreases to 0.5 wt.% (Supplementary

217 data 1). The HI decreases between 6 and 9 m (98 – 25 mg HC. g^{-1} TOC) and remains stable, until 55 m

218 where the HI increases again to reach 118 mg HC g^{-1} TOC at 68 m. The OI is relatively high (mean

219 around 180 mg O_2 g^{-1} TOC) between 6 and 9 m and remains stable until the depth of 45.84 m (around a

220 mean of 76 mg O_2 g^{-1} TOC). However, one pulse of OI can be observed at 21.3 m (117 mg CO_2 g^{-1}

221 TOC). Below 45.84 m the OI values decrease (37 to 48 mg O_2 g^{-1} TOC). The RE parameters measured

222 in Tégulines Clay of the AUB230 borehole allow discriminating three main parts corresponding to the

223 top (6 – 9 m), the center (10 – 45 m) and the bottom of the borehole (55 – 68 m). At the top of Tégulines

224 Clay, the HI/OI relationship is quite classical with an obvious anti-correlation: the HI decreases and OI

225 increases in this section demonstrating a classical oxidation profile (Marchand et al. 2008).

226 Tégulines Clay of the AUB1010 borehole (Fig. 3) are characterized by low TOC content at the surface

227 and then remains homogenous with values comprised between 0.3 % and 0.6 %. The HI is high at the

228 top (192 mg HC. g^{-1} TOC) and decreases rapidly at 3.31 m (81 mg HC. g^{-1} TOC). Deeper, the HI remains

229 homogenous (17 – 29 mg HC g^{-1} TOC). The HI value at 1.88 m is high (192 mg HC. g^{-1} TOC) as for

230 the soil sample (TPH1-1 0-30) revealing more immature well-preserved OM. The OI values are

231   extremely high at the surface (883 mg $CO_2.g^{-1}$ TOC and 912 mg $CO_2.g^{-1}$ TOC at 1.88 m and 3.31 m

232   respectively) due to low TOC content and probably the input of surficial pedogenetic OM. Deeper, the

233   OI decreases rapidly and remains relatively stable along with the profile (122 – 241 mg $CO_2.g^{-1}$ TOC).

234   The trends of the HI/OI ratios in Tégulines Clay of the AUB1010 and the AUB230 boreholes are similar.

235   Tégulines Clay OM of the three boreholes plot in type III OM field, revealing the terrestrial origin and/or

236   well-oxidized type II OM. Tégulines Clay OM of the borehole AUB240 shows intermediate OI and HI

237   values indicating the most preserved conditions of OM. Tégulines Clay OM of the AUB230 borehole is

238   a mixture of type II- and type III- OM, revealing 1) either the ratio of inherited marine OM (type II) and

239   terrestrial input (type III) or 2) a degradation process of marine OM allowing a shift from type II- OM

240   to an intermediate type with a decrease in the HI and a slight increase in the OI compared to the original

241   quality of the OM at the time of its deposition. Tégulines Clay of borehole AUB1010 shows oxygenated

242   OM revealing more oxic conditions resulting in a shift from type II or more terrestrial oxidized (Fig. 4).

243   3.1.2 T_{max} and shape of the pyrolysis S2 peak

244   The S2 signal delivered by the Rock-Eval pyrolysis is a spectrum that allows defining the rate of

245   pyrolysate hydrocarbons expressed as a function of temperature (Copard et al. 2006). Deconvoluting the

246   S2 signal permits us to better understand the evolution of the pyrolysis Temperature (T_{peak}) to unravel

247   the composition of the natural organic matter, which is generally composed of a complex mixture of

248   organic compounds. The S2 peak is non-Gaussian and is accompanied by shoulders for the immature

249   samples. The different peaks and shoulders correspond to the cracking of the different organic

250   compounds (Disnar 1982; Disnard & Trichet 1984; Disnar et al., 2003). The literature concerning the

251   shape of the pyrolysis S2 peak is mainly focused on soils samples. In this study, the different peaks of

252   OM in the soil sample (TPH1-1 0-30 cm) can be attributed to specific compounds. The S2 peak shows

253   a broad shape and two T_{peak} at 370 °C and 460 °C (C3 and C4) (Fig. 5a), typical of a soil sample and in

254   agreement with the bulk RE results. The cluster C3, at 370 °C can be attributed to the thermal breakdown

255   of biological constituents such as polysaccharides and lignin (Disnar et al. 2003). The C4 cluster shows

256   more preserved OM. For this sample, cluster C1 is absent. In their study, Copard et al. (2006) showed

257   that the C1 cluster (260 °C) is more labile and easily mineralized and could be easily absent in the most

258   diagenetically or pedogenetically evolved samples.

259   For OM in Tégulines Clay, the shape of the pyrolysis S2 peak does not permit to attribute a specific

260   compound but will permit to interpret the results in term of preservation. The mathematical

261   deconvolution of S2 peak show five molecular RE pyrolytic families named C1 to C5 with 260, 310,

262   370, 460 and 560 °C T_{peak} respectively (Fig. 5, 6 and supplementary data 2).

263   Tégulines Clay OM in AUB240 borehole shows very homogeneous cluster contribution with depth (Fig.

264   5b; Fig. 6a). C4 is the major cluster encountered (80 %), followed by C3 and C5. The distribution of

265   these contributions reveals preserved conditions with diagenetically well stabilized OM and are in

266   accordance with the bulk RE values (Copard et al. 2006).

267   Tégulines Clay OM in AUB230 and AUB1010 boreholes show variations of the cluster distribution with

268   depth. In AUB230 borehole, OM between 9 and 55 m show a high contribution of the C4 cluster (Fig.

269   5d, Fig. 6b supplementary data 2) that is almost similar to Tégulines Clay OM in AUB240 borehole,,

270   revealing stable OM input in probably good preserved conditions. At 21 m, the C2 cluster is more

271   represented indicating the presence of labile OM. At the top of the clay formation (6.10 m), OM is

272   particular with a high contribution of the C1 cluster (Fig. 5c). This could be due to the presence of light

273   recycled OM composed of a small molecular structure easily thermopyrolysable. At the bottom of the

274   clay formation (67 and 68 m) (Fig. 5e), the higher contribution changes to C3 cluster also revealing

275   stable and preserved OM (Copard et al. 2006).

276   Tégulines Clay OM in AUB1010 borehole (Fig. 5; Fig. 6c) shows an S2 deconvolution similar to that

277   in AUB230 borehole. The most upper sample (AUB1010 1.88, Fig. 5f) is characterized by the

278   contribution of C1, C3 and C4 (35, 45 and 20% respectively) clusters. The C1 cluster reveals the

279   presence of thermally labile biological compounds and shows more immature OM that could be, as for

280   the AUB230 6.10 m, a similar light recycled OM. Between 3 and 16 m, the major cluster is C4 (Fig. 5g,

281   h): stable OM with a variable contribution of the other clusters. Between 17 and 34 m (Fig. 5i), the major

282   cluster is C4, followed by C3 and C5. These conditions are similar to the AUB240 borehole and suggest

283   more stabilized and preserved OM.

284

285   The R400 parameter (proportion of the S2 peak integrated before 400°C, Disnar et al. 2003) and

286   depending on the proportion of labile and probably more diagenetically reactive biomolecules was also

287   calculated (supplementary data 1). This parameter varied between 0.1 and 0.6 and was higher for surface

288   samples (0.6 at 0-30 cm) indicating the presence of 60 % of labile OM in the surface. This parameter

289   was low in the AUB240 borehole (0.10 – 0.14) which is related to the 90 % of more stable OM (10 %

290   of labile OM) with highly refractory character.

291   T_{max} is also largely used in the literature in order to characterize the maturity of the OM. A general

292   overview of the samples reveal that the T_{max} is lower than 430 °C, suggesting that the OM is considered

293   immature.

294   3.2 Quantitative palynofacies investigations

295   The particles observed in the different samples were identified following the different morphological

296   and textural criteria presented in Fig. 2 and table 1. All the acronyms cited in the next section are detailed

297   in the table 1.

298   The quantitative palynofacies results for TPH1-1 are presented in Fig.7a. As expected from the Rock-

299   Eval results, the sample collected in the first 30 cm (0-30 cm) reveals a predominance of preserved

300   lignocellulosic fragments (plc), slightly degraded lignocellulosic fragments (slc) plc+slc (4.41 mg. g^{-1})

301   and divers particles (div) (1.70 mg.g^{-1}). The pyrite is absent at this depth. These lignocellulosic

302   compounds are, in their majority under gel-like forms, suggesting the sequestration of these particles in

303   an anoxic hydromorphic environment permitting protection artificially the OM (Boussafir et al 2012).

304   These parameters are in accordance with the RE data (high TOC, HI) and S2 deconvolution are typical

305   of a soil sample. The samples from the trench collected below 30 cm (30 cm to 5 m) did not permit to

306   perform any quantitative analysis due to the too-small number of residual particles in the palynofacies.

307   Tégulines Clay OM in AUB240 borehole (Fig. 7b) shows a homogeneous palynofacies content with

308   depth. The major particles encountered are the grAOM (1.11 – 2.31 mg.g^{-1}) followed by the OgAOM

309   (0.06 – 0.69 mg.g^{-1}) and do (0.26 – 0.51 mg.g^{-1}). OgAOM content increases between 29 and 80 m (0.06

310   mg.g^{-1} – 0.69 mg.g^{-1}) and pyrite is observed in inclusion. All these features suggest preserved anoxic

311   conditions of the initial deposit and agree with the RE and deconvolution results.

312   For the borehole AUB230 (Fig. 7c), at 6.10 m, the palynofacies is dominated by grAOM (1.03 mg.g^{-1}).

313   There is also the presence of pyrite (0.59 mg.g^{-1}) and od (0.27 mg.g^{-1}) with small particles (between 10

314   and 20 µm). In addition, the div category decreases in comparison with the surface. At 9.36 m, the

315   palynofacies is characterized by small particles (around 1 µm) and pyrite is absent. The presence of

316   small black particles as opaque-debris and/or oxidized Lignocellulosic particles suggests more oxidative

317   conditions. Between 10 and 18 m the grAOM is present in a higher proportion (between 1.47 and 4.51

318   mg.g^{-1}). The proportion of OgAOM is higher than the 9.36 m sample (between 0.090 and 0.24 mg.g^{-1}).

319   The od proportion is homogeneous in this depth range. At 25 m, the proportion of OgAOM increases

320   (0.35 mg.g^{-1}) and the pyrite content also increases (0.49 mg.g^{-1}). Between 30 and 55 m, the proportion

321   of grAOM is higher than the other samples (between 1.99 and 4.83 mg.g^{-1}) there is also the presence of

322   pyrite and the od category detains bigger size (~100 µm). At the end of the borehole, (55-68 m), the

323   proportion of grAOM is the highest (4.83-6.83 mg.g^{-1}), the OgAOM proportion is also high (0.57-0.84

324   mg.g^{-1}) with bigger size and pyrite in inclusion. The palynofacies show a higher contribution of grAOM

325   and OgAOM with pyrite inclusion. This feature also shows more preserved conditions. The increase of

326   the AOM particles is correlated with the increase of HI and the principal contribution of C3 cluster

327   suggesting that this AOM is the principal component of kerogen and suggest more preserved conditions

328   of the formation.

329   The palynofacies for the AUB1010 borehole was difficult to interpret because the particles were present

330   in very low proportion and could not permit any quantitative work. The particles were mainly composed

331   of very small (around 1 µm) OgAOM and od particles. The samples of the AUB1010 borehole are

332   similar to the AUB230 (6.10 m) sample and suggest more oxidative conditions.

333   The palynofacies is representative of the organic matter composition after the sedimentation and the

334   organic diagenesis (Tyson 1993, Zhang et al. 2015). The different assemblages of refractory particulate

335   organic matter permit to record environmental evolution and depositional characteristics. In particular,

336   the different distributions can reflect the conditions of the oxygenation (Tyson 1993, Disnar et al. 2003,

337   Di-Giovanni et al. 1999a). As mentioned in the geological setting, the Gault Clay was deposited in an

338   open marine environment (Lerouge et al. 2018). Indeed, the presence of Glauconie, Siderite and Pyrite

339   are characteristic of an anoxic marine deposition at shallow depth. In our study, AUB230 (at 55-68 m)

340   and the AUB240 samples present the well-preserved palynofacies assemblage. These samples show the

341   presence of AOM with pyrite in inclusion (Fig. 7b, c). (Tyson 1993, Boussafir et al 1995a, b) showed

342   that the presence of gel-like AOM is generally associated with high preservation rates and low energy

343   environments and result to anoxic deposits. This OM is similar to that observed in Kimmeridgian clays

344   Formation (Boussafir et al, 1995, a, b, Boussafir et al. 1997) and has an ultrafine monoscopically

345   amorphous structure derived from the preservation by natural sulfuration in an anoxic environment. The

346   H_2S produced during the sulphate-reduction process allows the formation of pyrite in association with

347   the iron present in the sediments and preserve a part of the initially metabolizable OM and therefore

348   becomes resistant to degradation and oxidation. This process is at the origin of the highly stabilized

349   nature of the OM of these clays. Consequently, the OM of Tégulines Clay is insensitive to

350   physicochemical conditions and would probably not have a direct action on the redox system of this

351   clay formation.

352

353   3.3 Molecular investigation in Tégulines Clay OM

354   3.3.1 Total lipids extract

355   Tégulines Clay samples from the AUB230 borehole were selected for the molecular investigation of

356   organic matter, based on S1 (> 0) and TOC values (~0.2) of the RE results.

357   The extract concentrations in Tégulines Clay are characterized by low content in labile compounds (0.3

358   to 1.0 mg.g^{-1} of dry sediment), and are consistent with the Rock-Eval quantitative (TOC) and qualitative

359   (HI and OI) parameters and the palynofaciès composition (supplementary data 1), indicating the

360   immaturity of OM (low free HC) and preserved insoluble kerogen. The extract concentrations in

361   Tégulines Clay samples from the AUB240 and AUB1010 boreholes are very low and close to 0 mg/g

362   (Rock-Eval ,S1, supplementary data 1), giving evidence of refractory and residual OM essentially.

363

364   3.3.2 Chromatograms patterns: n-alkanes

365   The molecular composition of the Tégulines Clay samples for the AUB230 borehole was investigated.

366   Three chromatograms patterns are presented in Figure 8 (sample at 6.10 m representing the oxidized

367   area, sample at 25 m and, sample at 66 m representing preserved area). Very few compounds are present

368   in the different samples. Phthalates compounds were found in the samples (55 – 60 min retention time).

369   the origin of these phthalates is unknown and could be the result of the extremely low concentration of

370   natural organic compounds in the samples that could exacerbate the phthalates peaks and are not related

371   to laboratory contamination. Several steroids were also encountered. In the biosphere, sterols detain

372   essentially 27, 28 and 29 C atoms. C_{27}-sterols produced by animals and C_{28}-sterols produced by

373   microalgae and fungi, C_{29}-sterols are synthesized by land plants (Huang and Meinschein 1979; Volkman

374   1986). The samples from the top and intermediate depths (6.10 m to 45 m) are composed of sitosterol,

375   sitostanol, cholesterol, cholestanol coprostanol and epi-coprostanol. These sterols have a terrigenous

376   origin. The end of the borehole is exempt from sterols.

377   This study mainly focuses on the alkanes composition in the different samples as they are more abundant

378   and can lead to several calculations such as the Carbon Preference Index (CPI). The n-Alkanes are

379   ubiquitous in the environment and are directly synthetized by living organisms or derived from straight-

380   chain biolipids (Eglinton and Hamilton, 1967). They can be used to discriminate the sources and the

381   preservation of the sedimentary immature OM (Brocks and Summons, 2003).

382   The total abundance of n-Alkanes varies between 0.29 and 9.14 µg/g sed, and increases from the bottom

383   to the top of the clay formation (Table 4). In the AUB230 borehole, n-alkanes were dominated by n-

384   C29 to n-C33 (Fig. 8) rather typical of terrestrial OM. The CPI defined by Bray and Evans, (1961) was

385   determined with the following equation: CPI = 2(odd n-C23 to n-C31) / (even n-C22 to n-C30 + even

386   n-C24 to n-C32). The n-alkanes CPI index is generally interpreted in terms of the origin. A CPI ~ 1

387   indicates marine origin, whereas a CPI > 1 reflects more terrestrial contribution. Between 9.36 and 45

388   m, the CPI value is ~1.0 suggesting more marine contribution, however, this value could also reflect the

389   oxidation of the OM. At the end of the borehole, the CPI is higher than 1, reflecting a mixture of marine

390   and terrestrial organic compounds, more representative of the sedimentation conditions. CPI can also be

391   used in order to characterize the degree of preservation of the n-alkanes in the sediments (Xie et al. 2004,

392   Zheng et al. 2007, Jansen and Nierop, 2009 Zhou et al. 2010; Garel et al., 2013). CPI values between 3

393   and 10 refer to preserved OM. Values between 1 to 3 are the first signs of early degradation. Values

394   close to 1 indicate more bacterial activity or recycled OM. At the start of the diagenesis, the molecular

395   compounds are mainly composed of oxygen functional groups. During the diagenesis, the

396   defunctionalization of the compounds leads at the end to the formation of hydrocarbons. The lipids that

397   are stocked in the sediments lead to the loss of many compounds and short chains molecules are more

398   degraded than the long chains ones.

399   The CPI values, calculated from the n-alkanes concentrations showed variations with depth. The CPI

400   was high for the trench sample and decreased after to values around 1 (9.36 – 21.30 meter deep). At the

401   end of the borehole, the CPI values increased again. These features suggest more preserved OM at the

402   top, in relation to the immature state of the OM, more degraded conditions between 9.36 and 21.30 m

403   and again, more preserved conditions (or slightly degraded) at the end of the borehole. These results are

404   in accordance with the RE and palynofacies results. The top of the AUB230 borehole is oxidized and

405   after 21 m, more preserved OM is observed. However, the CPI ratio shows oxidized conditions until 21

406   m whereas the palynofacies and at a lesser extent, the RE data shows an oxidation profile until 10 m.

407   The CPI ratio is in accordance with the mineralogical data (Lerouge et al. 2018) where the oxidation

408   profile is observed until 21 m.

409

410   3.4 Comparison with other marine clay formations – Impact of the oxidation
411

412   From a general overview, the TOC values show that the Tégulines Clay are very poor in organic content.

413   Guo et al. (2021) also studied the Tégulines clay in order to investigate the mobility of organic

414   compounds in this formation. Despite a low TOC content (as observed in this study), they observed the

415   retention of certain compounds such as lipophilic compounds. Other marine clay-rich formations that

416   have experimented low temperature such as Tégulines Clay have been extensively investigated in the

417   literature concerning their organic matter composition and variations. The Opalinus Clay from northern

418   Switzerland did not display a higher temperature of burial than 85 °C (Elie and Mazurek, 2008). They

419   also display quite low C contents from 0.1 to 1 wt% (Todorof et al. 1993; Nagra, 2002). Callovo-

420   Oxfordian claystones is another formation, located in the Eastern part of the Paris basin, that experienced

421   low temperature (50 °C) (Landais and Elie, 1999). Their total organic C content is also generally low

422   (<1 wt.% of the bulk rock). The T_{max} recorded for the Tégulines Clays is essentially < 430 °C. This

423   temperature is revealing immature OM. The RE T_{max} of the Opalinus Clay also displays temperatures

424 ≤435 °C in accordance with low thermal maturity. The thermal immaturity of the Callovo-Oxfordian

425 formations was demonstrated by the predominance of odd/even long-chain n-alkanes with CPI higher

426 than 2 (Hautevelle et al. 2007). In the case of the Tégulines Clay, the CPI cannot estimate the immaturity

427 as most of the formation is under oxidation. However, CPI can be used for the estimation of the

428 preservation. Our study emphases that the RE technique is suited to be used for oxidized formations.

429 The HI versus OI plot (pseudo Van Krevelen plot, Fig. 4) is usually employed to separate the marine

430 and terrestrial contributions in preserved conditions. In Elie and Mazurek (2008), the Opalinus Clay

431 falls into the Type III kerogen area, revealing more terrestrial contribution. The Callovo-Oxfordian

432 formations van Krevelen diagram indicate type II and III OM mixture, showing a marine origin, with a

433 contribution of terrestrial-derived materials (Disnar et al. 1996; Hautevelle et al. 2006). For the

434 Tégulines Clay, no conclusion permits to settle between marine or terrestrial contribution because the

435 HI and OI values can also suggest the presence of oxidized marine contribution, leading to the transfer

436 to the type III kerogen area.

437 The molecular investigation of the Tégulines Clay seems also to be perturbed by the oxidation profile.

438 The yields of OM extract in Tégulines Clay are low 0.3 to 1.0 mg. g^{-1} of dry sediment. By comparison,

439 the extract yield for Opalinus Clay is comprised of 0.9 and 48 mg. g^{-1} (Elie and Mazurek 2008). The

440 yield fractions of soluble OM ranges between 0.01 and 0.65 mg of organic extract/g of rock for the

441 Callovo-Oxfordian formations (Hautevelle et al. 2007). Despite the low yield of soluble OM, Callovo-

442 Oxfordian formations displayed a large variety of compounds deciphered by GCMS (n-alkanes, steroids,

443 hopanoids among others), permitting to get information on the OM maturity and origin. In contrast, the

444 chromatograms patterns of the different samples from the AUB230 borehole show the presence of a low

445 number of peaks, revealing a low number of molecular compounds (Fig. 8). Only n-alkanes could be

446 easily deciphered. However, the results concerning the n-alkanes distribution and the CPI are

447 questionable. Indeed, the predominant n-alkanes are ranging between C_{29} and C_{33}, revealing terrestrial

448 origin such as for the Opalinus Clay (Odd/Even predominance of C_{25}-C_{35} range (Elie and Mazurek,

449 2008)). By contrast, the Tegulines CPI is ~ 1 revealing marine origin. These opposite results could stem

450 from an artifact caused by the oxidation of the OM, shifting the short-chain of n-alkanes. These results

451 can question the use of certain techniques when dealing with oxidized OM.

452 3.5. Comparison of the TCF OM with mineralogical and dissolved inorganic carbon

453 (DIC) changes through the TCF weathering profile

454 In this study, the AUB230 borehole enabled to evidence the three main facies (from the bottom to the

455 top: UAQ, UA, and UAC units, see §2.1.) that can be encountered in the TCF, whereas the AUB1010

456 borehole only crosscut the UAQ and UA units (Lerouge et al., 2018). In the both boreholes, the oxidation

457 profile was observed between the sub-surface and ~21 m depth (Lerouge et al., 2018, 2020) (Fig. 9).

458 The brown and granulous textures, the bulk and molecular characteristics of the OM at the surface (0-

459 30 cm borehole AUB230) revealed high amounts of organic matter showing typical oxidative

460 degradation in soil, according to the following reaction: $CH_2O + O_2 = H_2O + CO_2$. These observations

461 are in good agreement with the DIC of 1.4 mEq/L measured in soil pore waters, the high CO_2 soil

462 degassing and the low $\delta^{13}C$ value of degassed CO_2 (-25.5 ‰ PDB) (Lerouge et al., 2020).

463 Between 30 cm and 5 m deep in the AUB230 borehole, in ocher carbonate-free sandy clay loams

464 overlying TCF, the bulk and OI index of the OM gave evidence of extremely low TOC contents and

465 high oxidative conditions consistent with the altered pedogenetic OM surficial bring (Fig. 4). These

466 observations are in good agreement with the low DIC (<0.9 mEq/L) measured in pore waters and the

467 low $\delta^{13}C$ values of DIC (~ -21 ‰ PDB) (Lerouge et al., 2020).

468 Below ~5 m in the AUB 230 borehole and ~2-3 m in AUB1010 borehole, the top of TCF is ocher, plastic

469 and marked by an intense and visible oxidation of pyrite and other iron-bearing minerals (iron-rich clays,

470 ankerite) that decreases down to 11 m depth. Pyrite oxidation leads to iron oxyhydroxide and gypsum

471 precipitation, but also to a small calcite dissolution due to slight acid pH. Ankerite oxidation leads to

472 iron oxyhydroxide precipitation. The clay fraction in TCF is quite homogeneous and composed by

473 ~16±5 % of detrital kaolinite, ~16±4 % of illite-smectite, ~12±5 % of illite-mica, and minor chlorite (<2

474 %), and ~8±6 % of diagenetic glauconite. The study of clay minerals in the 5-10 m zone, based on

475 microscopic observations, XRD and electron microprobe gave evidence of a change of color from

476 greenish to ocher due to oxidation of iron, a loss of iron to form iron oxides and an increase of the

477 smectite component, in particular concerning chlorite and glauconite (Lerouge et al. 2018, 2020). In the

478 same way, the OI of the OM is high and confirms oxidative conditions. Combined mineralogical and

479 OM data are consistent with the high DIC values (up to 8.5-8.6 mEq/L) measured in Tegulines Clay

480   pore waters in the 5-10 m zone of the both AUB230 and AUB1010 borehole. The $\delta^{13}C$ values of

481   degassed CO_2 (-19.5 to -12.9 ‰ PDB) corresponds to a mixing between OM matter degradation and

482   CO_2 due to calcite dissolution (Lerouge et al., 2020). The OM study gave a supplementary information

483   with the OI index, which is consistent with a mixing of the altered pedogenetic OM surficial supply and

484   the oxidation of original organo-clays fraction of the initial marine sediments (Fig. 4). The identification

485   of OM surficial supply down to ~9-10 m is in good agreement with the rare presence of small roots

486   down to 10-12 m in boreholes (Lerouge et al., 2020). The oxidation of pristine marine OM down to ~9-

487   10 m in the weathering profile is also an important point, which is a subject of debate for chemical

488   modelling of weathering profile in marine clay formations (Bao et al., 2017).

489   Between 9-10 m and 55 m, the OM oxidation state was homogenous and low, whereas changes of

490   consistency from plastic to hard and of mineralogy (slight oxidation of glauconite marked by yellowish

491   color) were still observed at ~ 20-25 m (Debure et al. 2018; Lerouge et al. 2018). The variation between

492   plastic/non plastic behavior of the TCF seems to not play a role for OM preservation.

493   The bottom of the TCF evolved under reducing conditions, and are characterized by an enrichment in

494   clay minerals, including glauconite and smectite (Lerouge et al., 2018). The OM data also showed more

495   preserved OM with higher HI, the microscopic data also show more preserved conditions with higher

496   grAOM and OgAOM contents with the inclusion of pyrite suggesting the role of bacterial sulphate

497   reduction in an anoxic sedimentary environment. Indeed, the association of pyrite with the amorphous

498   orange gel-like organic matter is interpreted as a non-biodegradable and stable organic matter preserved

499   by incorporation of sulfur by natural sulfurization (Boussafir et al. 1994, 1995, 1997).

500   At interface with the Greensand, TCF shows a drop of the TOC, S1, S2 and an increase of OI

501   (Supplementary data 1). The green sand detains coarser particles than the Tégulines Clay and could store

502   and/or preserve less OM.

503   Overall, the OM characterization (RE, palynofacies) of TCF in the different boreholes supports a well-

504   developed oxidation profile in the ~ 0-10 m and preservation of reduced conditions in the deeper parts,

505   in agreement with the previous mineralogical and geochemical studies. As for sulfur and iron oxidation

506   states, the oxidized or preserved state of the OM will finally help to redox regulation with depth in the

507   Tégulines Clay. Indeed, despite a similar TOC content all along the investigated boreholes, the

508 preservation of the organic matter and especially its reducing capacity will be one of the parameters that

509 might influence the mobility of sensitive-redox chemical elements (Debure et al. 2018, 2020). The small

510 amount of preserved, very little functionalized and unreactive OM and the refractoriness and stability

511 of OM of almost all the borehole samples studied plead for a slight influence of OM in the Tégulines in

512 a redox system.

513 Clay minerals, and particularly smectite, can physically protect the OM in these sediments (Hedges and

514 Oades 1997; Nelson et al. 1999, Drouin et al. 2010; Mahamat et al. 2016). The comparison with the

515 organic data (TOC, HI, OI) shows that we have, at the bottom of the borehole an increase of clay

516 minerals, including smectite / smectite-illite and glauconite, and an IH increase. Bruun et al. (2010)

517 stated that smectite have higher capacity to stabilize organic matter than illite due to higher specific

518 surface area and cation exchange capacity. All these information permits to state that the protection

519 of the organic matter at the bottom of the AUB230 borehole (66 – 68 m) can be the presence of

520 smectite in higher proportion.

521 The OM is preserved in the AUB240 borehole while it was more oxidized in the AUB1010 at least

522 between 3 and 16 m and also observed from mineral characterizations. The OM preservation is higher

523 in the AUB240 borehole, as a 12 m layer of Brienne Marls overlies it themselves covered by 8 m of

524 surficial layers (loess, clay sediments and carbonated alluvium). By contrast, the surficial layer in the

525 AUB230 borehole represents only 5 m and even less (3 m) in the AUB1010 borehole. Therefore,

526 meteoric water reaches faster the Tégulines in the AUB1010 and AUB230 boreholes. Finally, the

527 difference between the AUB230 and the AUB1010 borehole relies on their position in the valley. The

528 AUB230 borehole is located at the hilltop while the AUB1010 is located at the bottom where the water

529 can stream from the hills. The position of the AUB1010 borehole is therefore favorable to a higher

530 alteration compared to the other boreholes and all these characteristics explain the higher oxidation depth

531 observed for organic matter in that borehole.

532

Conclusion

533
534   This study investigated the OM composition of the Tégulines Clay formation using bulk, microscopic

535   and molecular techniques. All the profiles studied show that Tégulines Clay are poor in organic content

536   in general. The bulk results using RE analyses revealed that the OM of all clays studied samples was

537   immature. The RE parameters, deconvolution of S2 peak, R400, palynofacies and molecular

538   investigations were all positively correlated. Indeed, at the surface (TPH1-1 0-30), the OM showed

539   relatively high HI and TOC with a large amount of preserved particles revealing typical soil litter OM.

540   The deconvolution of the S2 peak curve showed a dominant contribution of the C3 cluster that is typical

541   of the breakdown of polysaccharides and lignin in the surface part of the studied profile. The other trench

542   samples collected below 30 cm showed very oxidized conditions (low TOC and high OI). The AUB240

543   borehole, from the bulk and microscopic investigation, revealed more preserved conditions, mainly due

544   to the overlaying of the Brienne marls and is presented as a reference borehole in term of OM

545   preservation. The investigation of the AUB230 borehole clearly showed an oxidation profile at the top

546   and more pristine, preserved and reductive conditions deeper. The AUB1010 borehole showed similar

547   conditions to the AUB230 borehole but a higher oxidation depth. These different oxidation depths could

548   be explained by the different spatial topological location of the boreholes. This study showed that the

549   Tégulines Clay OM is: very low in amount, stable in its preserved section, essentially residual and little-

550   sensitive to the biotic and abiotic degradation and thus would be very weakly reactive. The OM influence

551   would also be limited in a redox system supporting previous results obtained on the behavior of

552   sensitive-redox chemical elements. Finally, this is supported on the one hand by the small amount of

553   preserved, very little functionalized and unreactive OM and on the other hand, by the refractoriness and

554   stability of OM of almost all the borehole samples studied. This study also shows that a good set of

555   techniques permit to deal with the complex atmosphere / Geological formations interactions in the

556   critical zone.

557

563 **References**

564   Altmann, S., Tournassat, C., Goutelard, F., Parneix, J. C., Gimmi, T., & Maes, N. (2012). Diffusion-

565   driven transport in clayrock formations. Applied Geochemistry, 27(2), 463-478.

566   Bao, Z., Haberer, C. M., Maier, U., Amos, R. T., Blowes, D. W., & Grathwohl, P. (2017). Modeling

567   controls on the chemical weathering of marine mudrocks from the Middle Jurassic in Southern

568   Germany. Chemical Geology, 459, 1-12.

569   Battarbee, R.W., Kneen, M.J. (1982). The use of electronically counted microspheres in absolute diatom

570   analysis. Limnology and Oceanography 27, 184 – 188.

571   Boussafir M., Lallier-Vergès E., Bertrand P. & Badaut-Trauth D. (1994). Structure ultrafine de la

572   matière organique des roches mères du Kimméridgien du Yorkshire. Bulletin de la Société Géologique

573   de France, 165, (4) 355-363.

574   Boussafir, M., Gelin, F., Lallier-Vergès, E., Derenne, S., Bertrand, P., & Largeau, C. (1995a). Electron

575   microscopy and pyrolysis of kerogen from the Kimmeridgien Clay Formation, UK: Source organisms,

576   preservation processes, and origin of the microcycles. Geochimica et Cosmochimica Acta 59, 3731-

577   3747.

578   Boussafir M., Lallier-Verges E., Bertrand, P., & Badaut-Trauth, D. (1995b). SEM and TEM studies on

579   isolated organic matter and rock microfacies from a short-term organic cycle of the Kimmeridge Clay

580   Formation (Yorkshire, GB), Organic matter accumulation, Springer, Berlin, Heidelberg , 15-30.

581   Boussafir, M., Lallier-Vergès, E. (1997). Accumulation of Organic Matter in the Kimmeridge Clay

582   Formation (KCF): An Update Fossilisation Model for Marine Petroleum Source-Rocks. Marine and

583   Petroleum Geology, 14 (1), 75–83.

584   Boussafir, M., Sifeddine, A., Jacob, J., Foudi, M., Cordeiro, R. C., Albuquerque, A. L. S., ... & Turcq,

585   B. (2012). Petrographical and geochemical study of modern lacustrine sedimentary organic matter

586   (Lagoa do Caçò, Maranão, Brazil): Relationship between early diagenesis, organic sedimentation and

587   lacustrine filling. Organic Geochemistry, 47, 88-98.

588   Bray, E.E., Evans, E.D. (1961). Distribution of n-paraffins as a clue to recognition of source beds.

589   Geochimica et Cosmochimica Acta 22, 2–15.

590   Brocks, J.J., Summons, R.E. (2003). Sedimentary hydrocarbons, biomarkers for early life. In: Holland,

591   H.D., Turekian, K. (Eds.), Treatise in Geochemistry, vol.8. Elsevier, Amsterdam, pp. 63 – 115.

592   Bruun, T. B., Elberling, B., & Christensen, B. T. (2010). Lability of soil organic carbon in tropical

593   soils with different clay minerals. Soil Biology and Biochemistry, 42(6), 888-895.

594   Combaz, A. (1964). Les palynofaciès, Revue de micropaléontologie 7, 205 – 218.

595   Combaz, A. (1980). Les kérogènes vus au microscope. In : Durant, B. (Ed.) Kerogen. Technips, Paris,

596   pp. 55 – 111.

597   Copard, Y., Di-Giovanni, C., Martaud, T., Albéric, P., & Olivier, J.E. (2006). Using Rock-Eval 6

598   pyrolysis for tracking fossil organic carbon in modern environments: implications for the roles of erosion

599   and weathering. Earth Surface Processes and Landforms 31, 135 – 153.

600   Debure, M., Tournassat, C., Lerouge, C., Madé, B., Robinet, J. C., Fernández, A. M., & Grangeon, S.

601   (2018). Retention of arsenic, chromium and boron on an outcropping clay-rich rock formation (the

602   Tégulines Clay, eastern France). Science of The Total Environment, 642, 216-229.

603   Debure, M., Grangeon, S., Robinet, J. C., Madé, B., Fernández, A. M., & Lerouge, C. (2020).

604   Influence of soil redox state on mercury sorption and reduction capacity. Science of The Total

605   Environment, 707, 136069.

606   Deniau, I., Devol-Brown, I., Derenne, S., Behar, F., & Largeau, C. (2008). Comparison of the bulk

607   geochemical features and thermal reactivity of kerogens from Mol (Boom Clay), Bure (Callovo–

608   Oxfordian argillite) and Tournemire (Toarcian shales) underground research laboratories. Science of

609   the Total environment, 389(2-3), 475-485.

610   Di–Giovanni, C., disnar, J.R., Bichet, V., & Campy, M. (1998). Sur la présence de matière organique

611   méso-cénozoïque dans les humus actuels (bassin de Chaillexon, Doubs, France). Comptes Rendus de

612   l'Académie des Sciences Paris, 326, 553 – 559.

613   Di-giovanni, C., Disnar, J.R., Campy, M., & Macaire, J.J. (1999a). Variability of the ancient organic

614   supply in modern humus. Analysis 27, 398 – 402.

615   Disnar, J.R. (1982). Etude expérimentale de la fixation de divers métaux sur une matière organique

616   sédimentaire d'origine algaire. Maturation thermique des composés formés. Thèse d'Etat, Université

617   d'Orléans.

618   Disnar, J.R., Trichet, J. (1984). The influence of various divalent cations (UO22+, Cu2+, Pb2+, Co2+,

619   Ni2+, Zn2+, Mn2+) on thermally induced evolution of organic matter isolated from an algal mat.

620   Organic Geochemistry 6, 865 – 874.

621   Disnar, J. R., Le Strat, P., Farjanel, G., & Fikri, A. (1996). Sédimentation de la matière

622   organique dans le nord-est du Bassin de Paris: conséquences sur le dépôt des argilites carbonées

623   du Toarcien inférieur (Organic matter sedimentation in the northeast of the Paris Basin:

624   consequences on the deposition of the lower toarcian black shales). Chemical geology, 131(1-

625   4), 15-35.

626   Disnar, J.R., Guillet, B., Keravis, D., Di-Giovanni, C., & Sebag, D. (2003). Soil organic matter (SOM)

627   characterization by Rock-Eval pyrolysis : scope and limitations. Organic Geochemistry 34, 327 – 343.

628   Drouin, S., Boussafir, M. Robert, J.L., Albéric P. & Durand, A. (2010). Carboxylic acid sorption on

629   synthetic clays in sea water: In vitro experiments and implications for organo-clay behaviour under

630   marine conditions. Organic Geochemistry 10.1016/j.orggeochem.2009.10.006.

631   Duffy, C., Shi, Y., Davis, K., Slingerland, R., Li, L., Sullivan, P. L.& Brantley, S. L. (2014).

632   Designing a suite of models to explore critical zone function. Procedia Earth and Planetary Science,

633   10, 7-15.

634   Eglinton, G., Hamilton, R. J. (1967). Leaf epicuticular waxes. Science, 156 (3780), 1322-1335.

635   Elie, M., Faure, P., Michels, R., Landais, P., & Griffault, L. (2000). Natural and laboratory oxidation

636   of low-organic-carbon-content sediments: comparison of chemical changes in hydrocarbons. Energy &

637   Fuels, 14 (4), 854-861.

638   Elie, M., Mazurek, M. (2008). Biomarker transformations as constraints for the depositional

639   environment and for maximum temperatures during burial of Opalinus Clay and Posidonia Shale in

640   northern Switzerland. Applied Geochemistry, 23 (12), 3337-3354.

641   Espitalié, J., Deroo, G., & Marquis, F. (1985a). La pyrolyse Rock-Eval et ses applications.Oil&Gas

642   Science and Technology, 40, 563 – 579.

643   Espitalié, J., Deroo, G., & Marquis, F. (1985b). La pyrolyse Rock-Eval et ses applications. Oil & Gas

644   Science and Technology 40, 755 – 783.

645   Garel, S., Schnyder, J., Jacob, J., Dupuis, C., Boussafir, M., Le Milbeau, C., Storme, J.Y., Iakovleva,

646   A.I., Yans, J., Baudin, F., Fléoch, C., & Quesnel, F.(2013). Paleohydrological and paleoenvironmental

647   changes recorded in terrestrial sediments of the Paleocene–Eocene boundary (Normandy, France).

648   Palaeogeography, Palaeoclimatology, Palaeoecology 376, 184–199.

649   Graz, Y., Di-Giovanni, C., Copard, Y., Laggoun-Défarge, F., Boussafir, M., Lallier-Vergès, E., Baillif,

650   P., Perdereau, L., & Simmoneau, A. (2010). Quantitative palynofacies analysis as a new tool to study

651   transfers of fossil organic matter in recent terrestrial environments. International Journal of Coal

652   Geology 84, 49 – 62.

653   Guo, N., Disdier, Z., Thory, É., Robinet, J. C., & Dagnelie, R. V. (2021). Mobility of organic compounds

654   in a soft clay-rich rock (Tégulines clay, France). Chemosphere, *275*, 130048.

655   Hautevelle, Y., Michels, R., Malartre, F., & Trouiller, A. (2006). Vascular plant biomarkers as proxies

656   for palaeoflora and palaeoclimatic changes at the Dogger/Malm transition of the Paris Basin (France).

657   Organic Geochemistry, 37(5), 610-625.

658   Hautevelle, Y., Michels, R., Malartre, F., Elie, M., & Trouiller, A. (2007). Tracing of variabilities within

659   a geological barrier by molecular organic geochemistry. Case of the Callovo-Oxfordian sedimentary

660   series in the East of the Paris Basin (France). Applied Geochemistry 22, 736 – 759.

661   Hedges, J.I, Oades, J.M. (1997). Comparative organic geochemistries of soils and marine sediments.

662   Organic Geochemistry 27, 319-361.

663   Hendry, M. J., Wassenaar, L. I., & Kotzer, T. (2000). Chloride and chlorine isotopes (^{36}Cl and δ^{37}Cl)

664   as tracers of solute migration in a thick, clay-rich aquitard system. Water Resources Research, 36(1),

665   285-296.

666 Huang, W. Y., & Meinschein, W. G. (1979). Sterols as ecological indicators. Geochimica et

667 cosmochimica acta, 43(5), 739-745.

668 Mahamat, A. M., Boussafir, M., Le Milbeau, C., Guegan, R., Valdes, J., Guinez, M., Sifeddine, A., &

669 Le Forestier, L. (2016). Organic matter-clay interaction along a seawater column of the Eastern Pacific

670 upwelling system (Antofagasta bay, Chile): Implications for source rock organic matter preservation.

671 Marine Chemistry doi:10.1016/j.marchem.2016.01.003

672 Lafargue, E., Marquis, F., & Pillot, D. (1998). Rock-Eval 6 applications in hydrocarbon exploration,

673 production and soil contamination studies. Revue de l'Institut Français du Pétrole 53, 421 – 437.

674 Jacob, J., Disnar, J.-R., Boussafir, M., Sifeddine, A., Albuquerque, A.L.S., & Turcq, B. (2005).

675 Pentacyclictriterpenemethylethers in recentlacustrinesediments (Lake Caço, Brazil). Organic

676 Geochemistry 36, 449–461.

677 Jansen, B., & Nierop, K.G.J. (2009). Methyl ketones in high altitude Ecuadorian Andosols confirm

678 excellent conservation of plant-specific n-alkane patterns. Organic Geochemistry 40, 61–69.

679 Landais, P., & Elie, M. (1999). Utilisation de la géochimie organique pour la détermination du

680 paléoenvironnement et de la paléothermicité dans le Callovo-Oxfordien du site de l'Est de la France.

681 EDP Sciences, 1999, 35-58.

682 Landais, P., Michels, R., Kister, J., Dereppe, J. M., & Benkhedda, Z. (1991). Behavior of oxidized

683 type II kerogen during artificial maturation. Energy & fuels, 5(6), 860-866.

684 Lerouge, C., Debure, M., Henry, B., Fernandez, A. M., Blessing, M., Proust, E., & Robinet, J. C.

685 (2020). Origin of dissolved gas (CO2, O2, N2, alkanes) in pore waters of a clay formation in the

686 critical zone (Tégulines Clay, France). Applied Geochemistry, 116, 104573.

687 Lerouge, C.,Robinet, J.C., Debure, M., Tournassat, C., Bouchet, A., Maria Fernandez, A., Flehoc, C.,

688 Guerrot, C., Kars, M., Lagroix, F., Landrein, P., Madé, B., Negrel, P., Wille, G., & Claret, F. (2018). A

689 deep alteration and oxidation profile in a shallow clay aquitard : example of the Tégulines Clay, East

690 Paris basin, France. Geofluidshttps://doi.org/10.1155/2018/1606753.

691

692   Marchand, C., Lallier-Vergès, E., Disnar, J. R., & Kéravis, D. (2008). Organic carbon sources and

693   transformations in mangrove sediments: a Rock-Eval pyrolysis approach. Organic Geochemistry,

694   39(4), 408-421.

695   Nagra. 2002. Project Opalinus Clay. Safety Report. Nagra Technical Report NTB 02-05. Nagra,

696   Wettin-gen, Switzerland.

697   Nelson, P. N., Baldock, A., Oades, J. M., Churchman, G. J., & Clarke, P. (1999). Dispersed clay and

698   organic matter in soil: their nature and associations. Soil Research, 37(2), 289-316.

699   Sebag, D., Di-Giovanni, C., Ogier, S., Mesnage, V., Laggoun-Défarge, F., & Durand, A (2006a).

700   Inventory of sedimentary organic matter in modern wetland (Marais Vernier, Normandy, France) as

701   source –indicative tools to study Holocene alluvial deposits (Lower Seine Valley, France). International

702   Journal of Coal Geology 67, 1 – 16.

703   Sebag, D., Copard, Y., Di-Giovanni, C., Durant, A., Laignel, B., Ogier, S., & Lallier-Verges, E. (2006b).

704   Palynofacies as useful tool to study origins and transfers of particulate organic matter in recent terrestrial

705   environments : synopsis and prospect. Earth Science Reviews 79, 241 – 259.

706   Todorov, I., Schegg, R. A., & Wildi, W. (1993). Thermal maturity and modelling of Mesozoic

707   and Cenozoic sediments in the south of the Rhine Graben and the Eastern Jura (Switzerland).

708   Eclogae Geologicae Helvetiae, 86(3), 667-692.

709   Tyson, R. V. (1993). Palynofacies analysis. In Applied micropalaeontology (pp. 153-191). Springer,

710   Dordrecht.

711   Tyson, R.V. (1995). Sedimentary organic matter: organic facies and palynofacies. Chapman and Hall,

712   London. 615 pp.

713   Vernal, A., Larouche, A., & Richard, J.H. (1987). Evaluation of palynomorph concentrations: do the

714   aliquot and the marker-grain methods yield comparable results? Pollen and spores XXIX, 291 – 304.

715   Volkman, J. K. (1986). A review of sterol markers for marine and terrigenous organic matter. Organic

716   geochemistry, 9(2), 83-99.

717

718   Xie, S., Nott, C., Avsejs, L., Maddy, D., Chambers, F., & Evershed, R. (2004). Molecular and isotopic

719   stratigraphy in an ombrotrophic mire for paleoclimate reconstruction. Geochimica et

720   CosmochimicaActa 68, 2849–2862.

721   Zhang, M., Ji, L., Wu, Y., & He, C. (2015). Palynofacies and geochemical analysis of the Triassic

722   Yanchang Formation, Ordos Basin: Implications for hydrocarbon generation potential and the

723   paleoenvironment of continental source rocks. International Journal of Coal Geology, 152, 159-176.

724   Zheng, Y., Zhou, W., Meyers, P.A., & Xie, S. (2007). Lipid biomarkers in the Zoigê-Hongyuan peat

725   deposit: indicators of Holocene climate changes in West China. Organic Geochemistry 38, 1927– 1940.

726   Zhou, W., Zheng, Y., Meyers, P.A., Jull, A.J.T., & Xie, S. (2010). Postglacial climate-change record in

727   biomarker lipid compositions of the Hani peat sequence, Northeastern China. Earth and Planetary

728   Science Letters 294, 37–46.

729

730

731

1   Table 1 *Characteristics of the different particles encountered in the different samples*

Classes	Categories	Characteristics
Amorphous particles	GrAOM: granular Amorphous Organic Matter	Diffuse limits, grey to yellow in transmitted light, opaque or slight orange in reflected light, size: 10-100 µm
	gAOM: Gelified Amorphous Organic Matter	Particle entirely gelified, no internal structure, orange to red in transmitted light, dark orange in reflected light, size: can reach very large size over 100 µm
	Gd: Gelified debris	Sharp contours, high reflectance, size: 10 µm
	Od: Opaque debris	Sharp contours, high reflectance, dark in transmitted light, size: 10 µm
Ligno cellulosic debris	Plc: Preserved lignocellulosic	Elongated particles with visible internal structures, yellow in transmitted light (10-100 µm)
	Salc: Slightly amorphised lignocellulosic	Elongated particles with visible internal structures, yellow to orange in transmitted light (10-100 µm), trace of gelification
	Glc: Gelified lignocellulosic	Elongated particles with visible internal structures, yellow to orange in transmitted light (10-100 µm), higher state of gelification
	Olc: Opaque lignocellulosic	No internal structure visible, elongated, show high reflectance (10-100 µm)
Other organic particles	Div: divers	Mycelium fragments: elongated particles, brown color; Cuticular fragments: particles with homogeneous limits, brown, with typical botanic structures, size variable and can exceed several hundred µm; Spores and pollens: particles from the terrestrial and aquatic flora, translucent or yellow for fresh particles and brown-orange for preserved particles; acritarchs, foraminifera
	pyrite	framboidal, opaque, with geometrical forms under transmitted light

2

3 Table 2 *Distributions, abundances and ratios of n-alkanes in the Trench TPH1-1 (0 – 30 cm sample) and AUB230 borehole.*
4 *[a]Majors n-alkanes in core samples, [b]Total = total abundance of n-alkanes (μg/g sediment), [c] odd/even ratio (odd/even =*
5 *∑conc. odd alkanes /∑conc. even n-alkanes) [d]n-alkanes carbon preference index CPI = 2(odd n-C23 to n-C31)/(even n-C22 to*
6 *n-C30+ even n-C24 to n-C32).*

7

	Major alkanes[a]	Total of alkanes (μg/g sed)[b]	odd/even[c]	CPI[d]
TPH1-1 0-30cm	n-C29, n-C31, n-C33	5.08	2.97	4.95
AUB230 9.36m	n-C29, n-C31, n-C33	9.14	1.26	1.08
AUB230 21.30m	n-C29, n-C31, n-C33	0.95	1.06	0.97
AUb230 25.32m	n-C29, n-C29, n-C31	0.61	1.37	1.19
AUB230 45.84m	n-C29, n-C31, n-C33	0.56	1.34	1.15
AUB230 66.35m	n-C29, n-C31, n-C33	0.47	0.97	1.57
AUB230 67.45m	n-C25, n-C31, n-C31	0.29	1.27	1.74

8
9
10
11
12
13
14
15
16
17
18
19
20
21
22
23
24

1 Fig. 1 (a) Geological map of the east part of the Paris Basin showing the studied area; (b) Geological map of the studied area
2 showing the location of the AUB240, AUB230 and AUB1010 boreholes selected for the organic matter study; (c) Major
3 mineralogy of the Tégulines clay from the AUB230 and AUB1010 boreholes deduced from XRD data treatment, compared
4 with previous data of AUB111 and AUB121 boreholes (Lerouge et al., 2018); UA: clay rich unit; UAC: carbonate-clay rick
5 unit; UAQ: clay-quartz rich unit
6

7

8

9

10

11

12
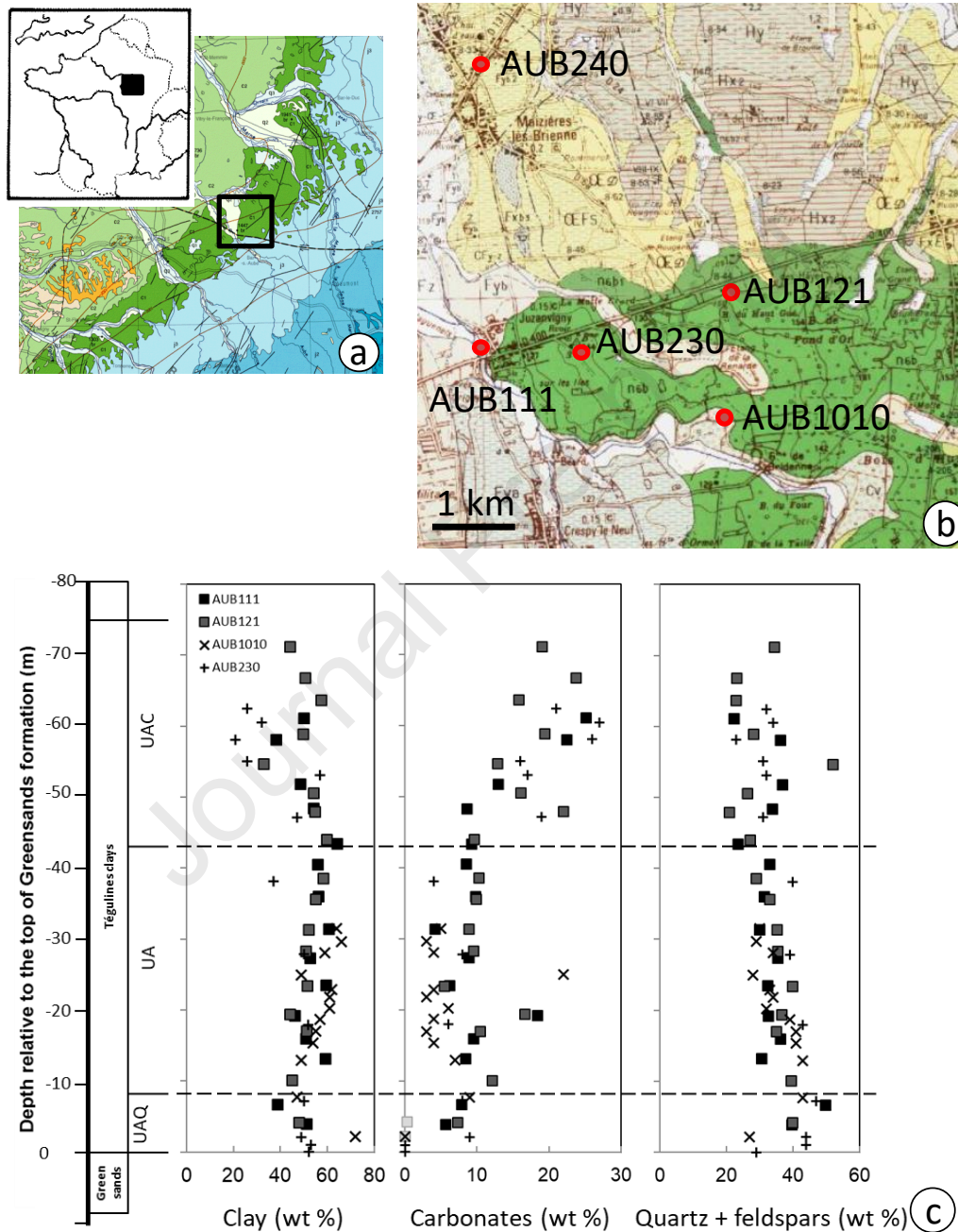
Fig. 2 The different categories of particulate organic matter distinguished from their morphology, the scale of the white bars corresponds to 100 µm; **Ligno-cellulosic fragments:** - preserved ligno-cellulosic fragments (plc),- slightly degraded ligno-cellulosic fragments (slc), - gelified ligno-cellulosic fragments (glc),- opaque ligno-cellulosic fragments (olc); **amorphous particles:** - granular amorphous organic matter (grAOM),- gelified amorphous organic matter (gAOM),- gelified debris (gd),- opaque debris (od) **Others organic particles:** - mycelium fragments (Myc); - foraminifera, - cuticular fragments (Cut), - Spores and pollens (sp), - (c) Pyrite.
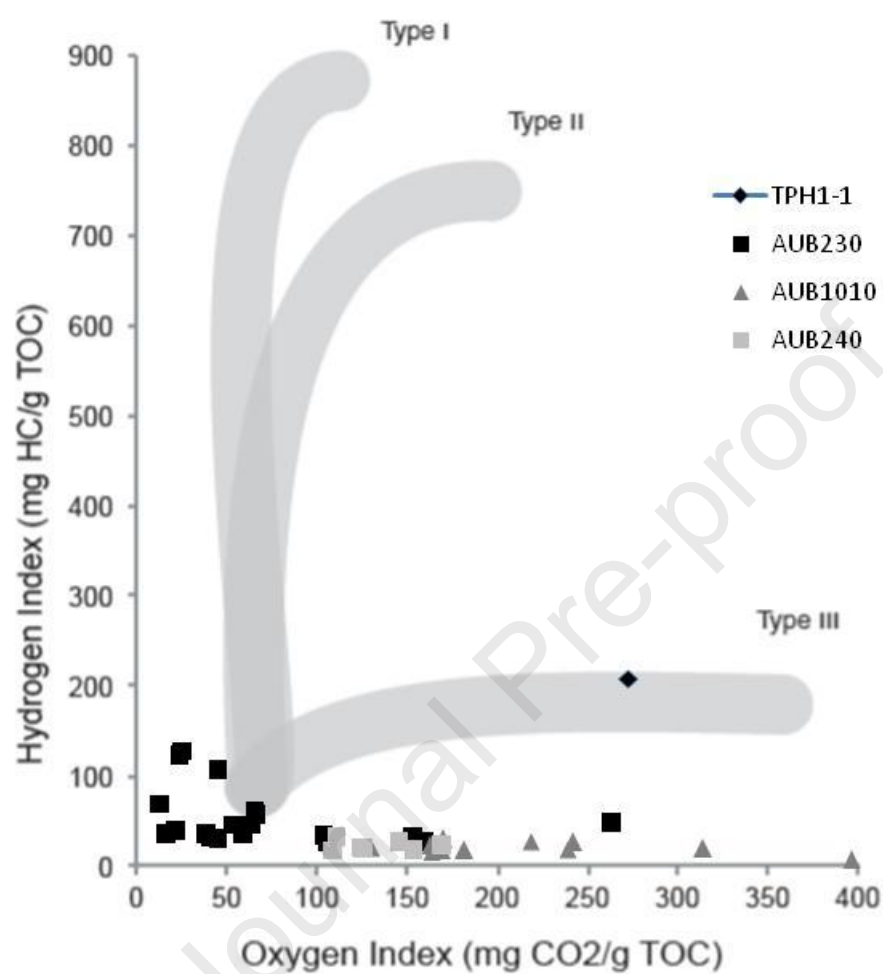

20

21

22

23

24

25
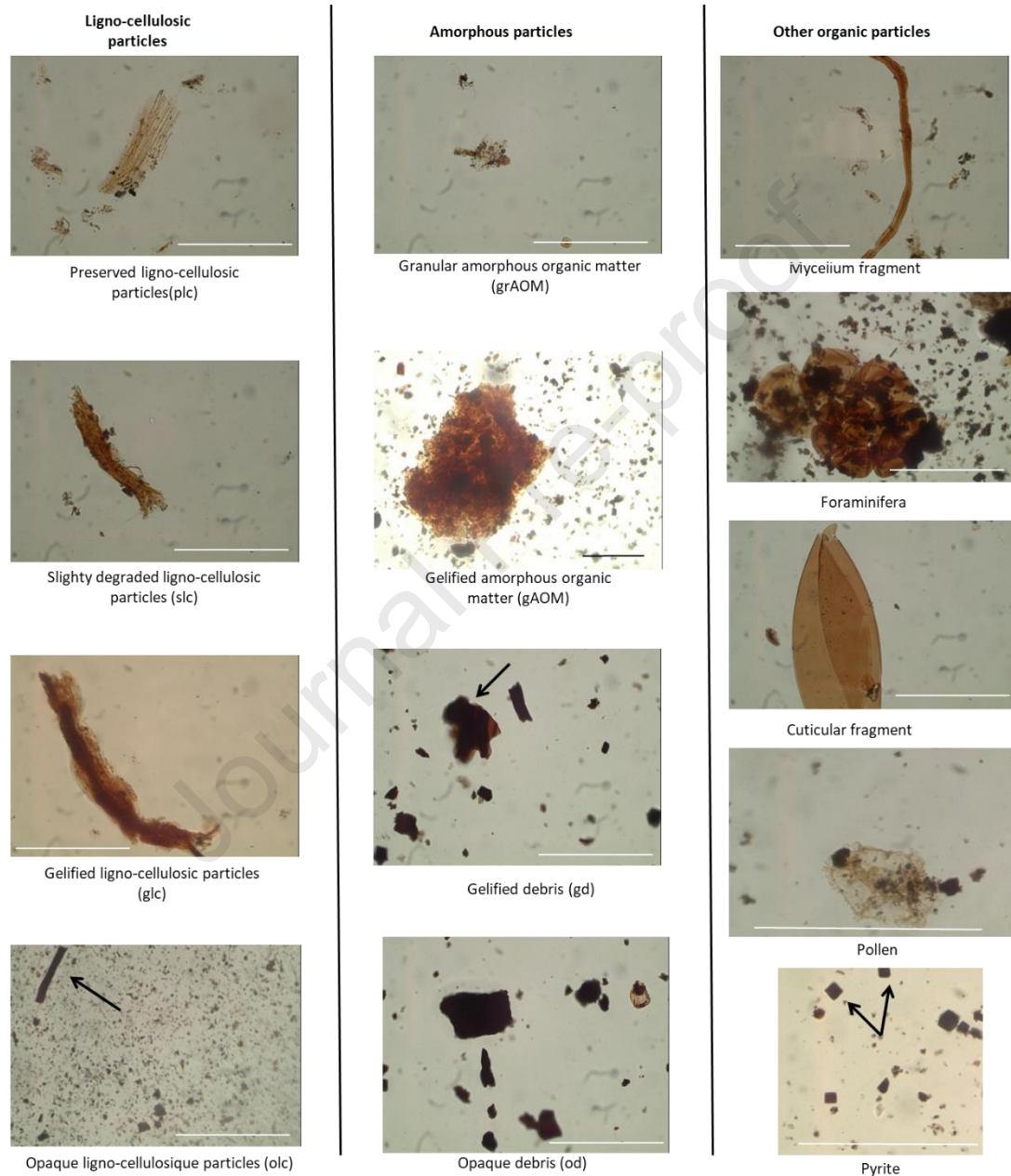
26 Fig. 3 Total Organic Carbon (TOC, %), Hydrogen Index (HI, *mg HC.g⁻¹TOC*), and Oxygen Index (OI, *mg CO2.g⁻¹TOC*) in
27 relation with depth for the AUB240, AUB230 and AUB1010 boreholes.
28

29

30

31

32

33

34

35

36

37

38

39

40

41

42

43

44

45

46

47

48
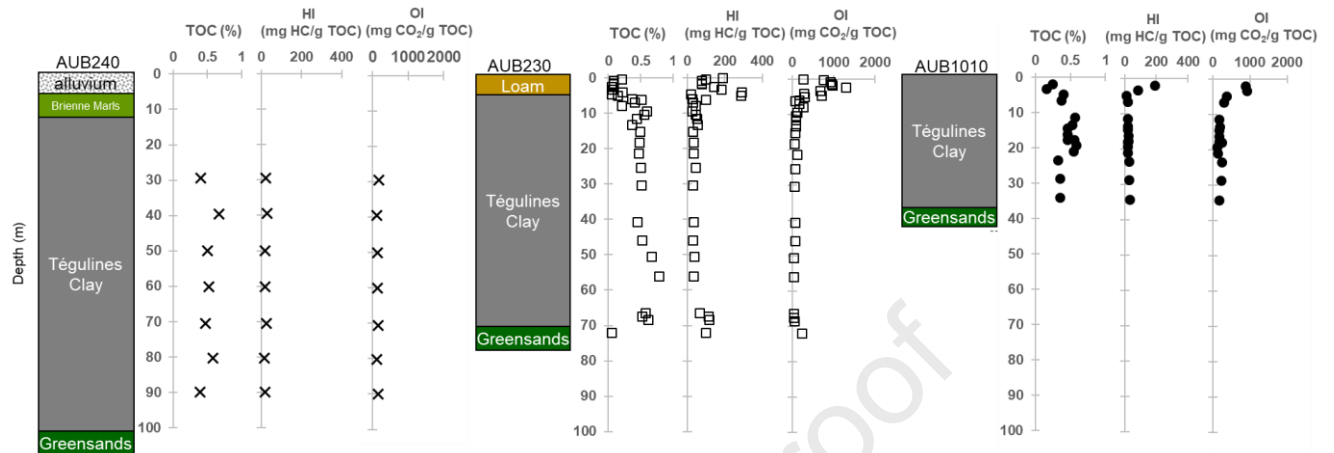
49

50   Fig. 4 Pseudo van-Krevelen diagram type for the different samples.
51

52
53

54

55

56

57

58

59

60

61

62

63

Fig. 5 Deconvolution of multilobed S2 signals from RE pyrolysis for *a TPH1-1 030 (r^2 = 0.996), b AUB240 39 (r^2 = 0.999), c AUB230 6.10 (r^2 = 0.994), d AUB230 25.32 (r^2 = 0.997), e AUB230 67.45 (r2 = 0.998), f AUB1010 1.88 (r^2 = 0.974), g AUB1010 3.31 (r^2 = 0.996), h AUB1010 14.47 (r^2 = 0.998), i AUB1010 20.95 (r^2 = 0.995). Black-grey curves are the rebuilt S2 signal from deconvolution.*

69
70

71

72
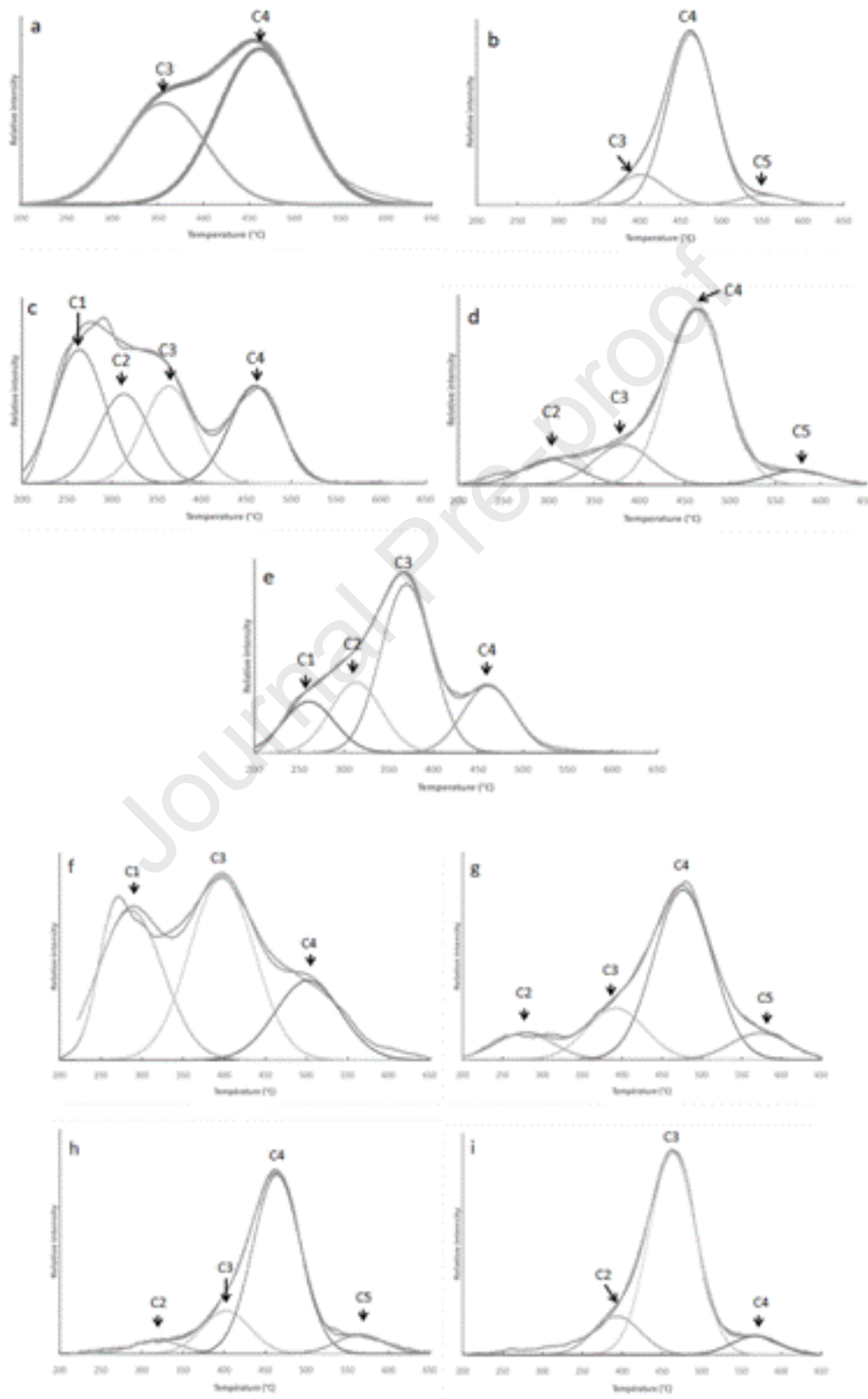
Fig. 6 *Contribution of the different clusters (C1-C5, %) AUB240, AUB230 and AUB1010 samples*

74

75
76

77

78

79

80

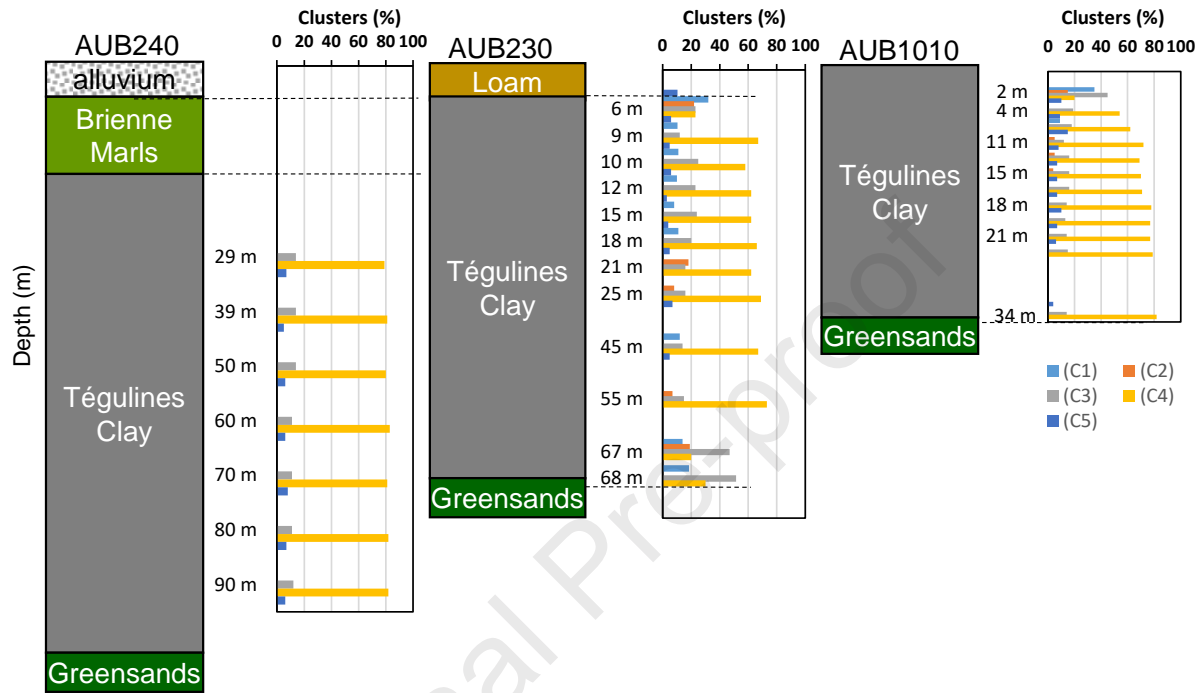81

82

83

84

85

86

87

88

89

90 Fig. 7 *Distribution of the different particles in: (a) TPH1-1 0-30 sample; (b) AUB240 borehole (29,39,70 and 80 m*
91 *deep); (c) AUB230 borehole (6.10, 18.22, 25.32, 45.84, 67.45 m and comparison with the TPH1-1 0-30)*
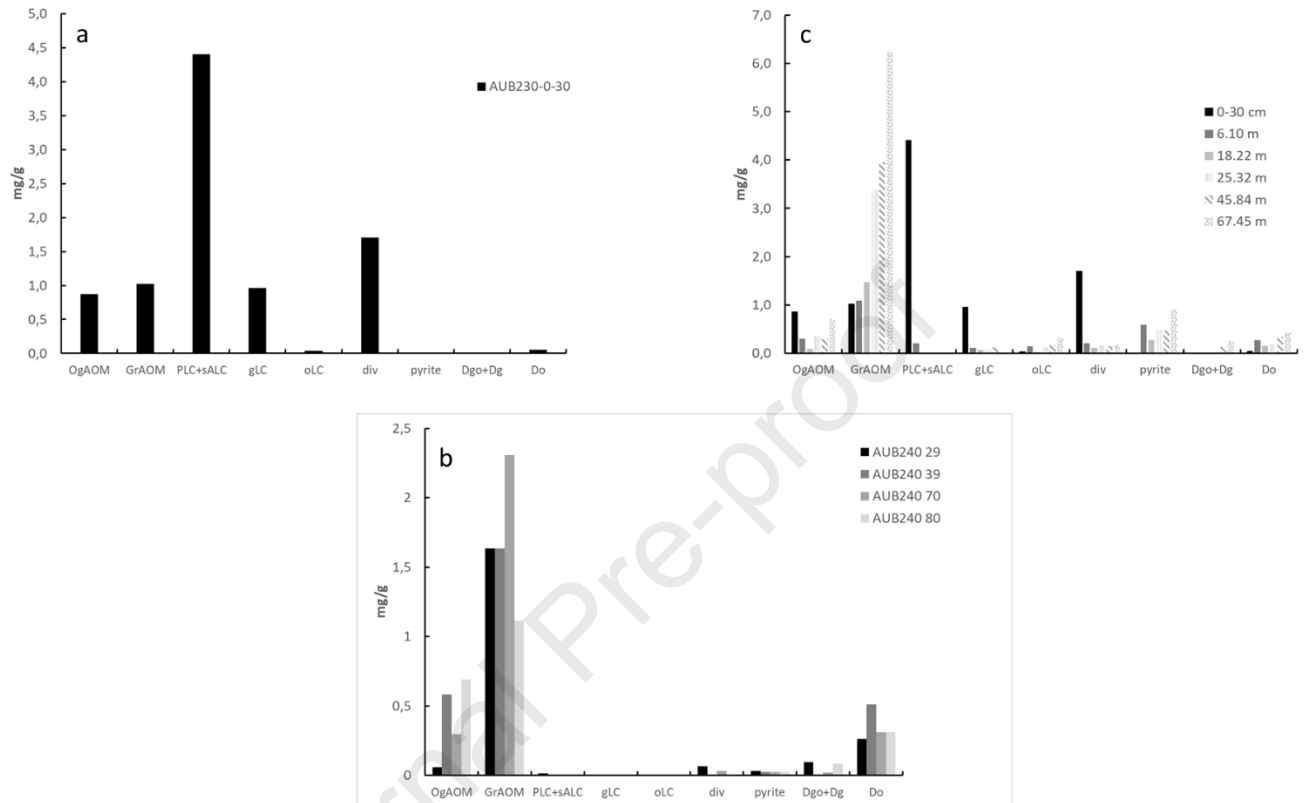
92

93
94
95
96
97
98
99
100
101
102
103
104
105
106
107

108

109

110   Fig. 8 *Chromatograms of the Tégulines Clay formation at 67 m; 25 m and 6.10 m*

111

112

113

114

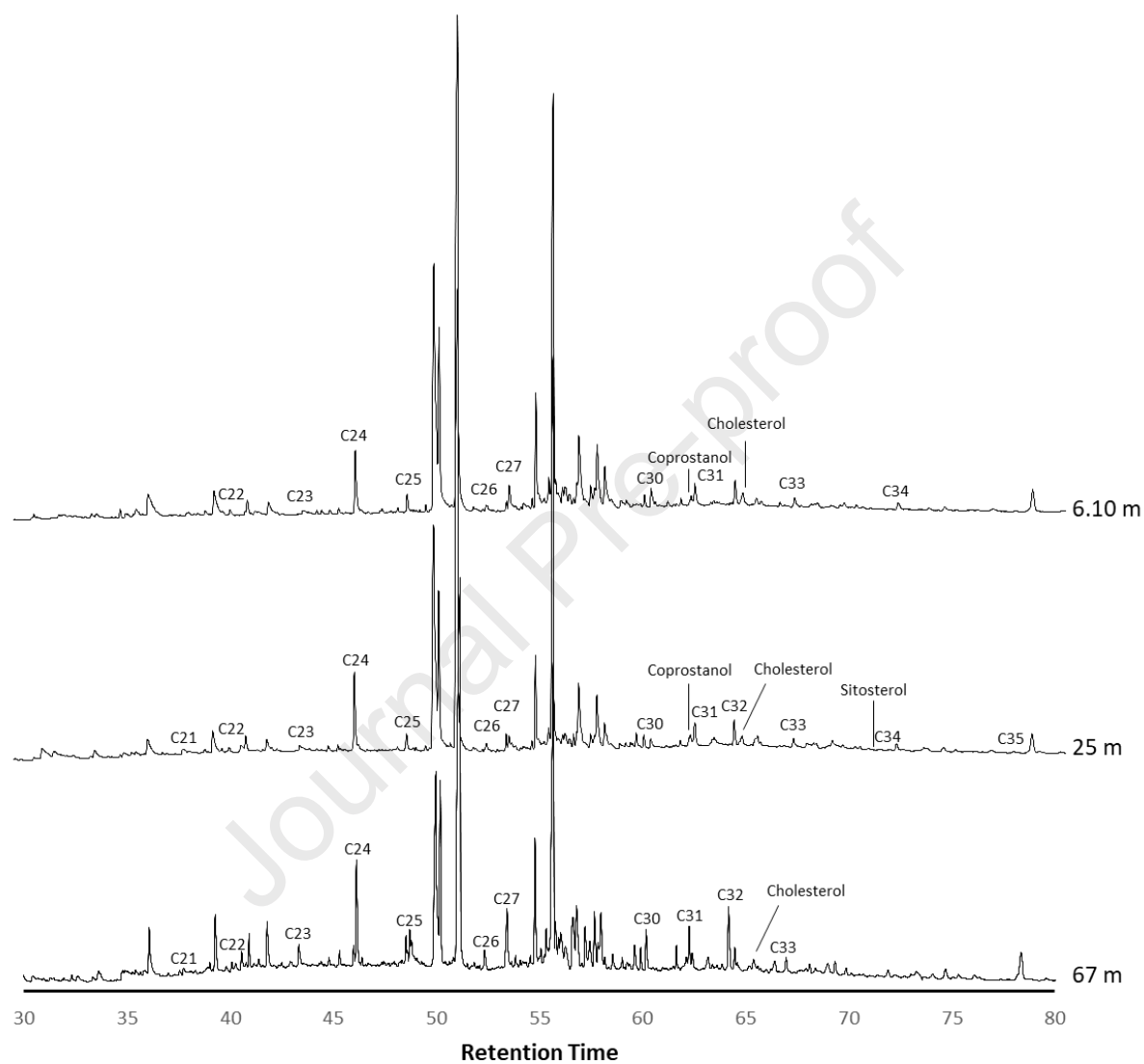115

116

117

118

119

120

121

122

123 *Fig. 9 Main characteristics of the organic matter through the weathering profile developed in Tégulines clay,*
124 *compared with mineral changes (Lerouge et al., 2018), dissolved inorganic carbon concentration (DIC) in pore*
125 *waters (PW) and contribution of degradation of organic matter (OM) to the DIC (Lerouge et al., 2020).*

126

127

128

129

130

131

132

133

134

135

136

137

138

139

140

141

142

143

144
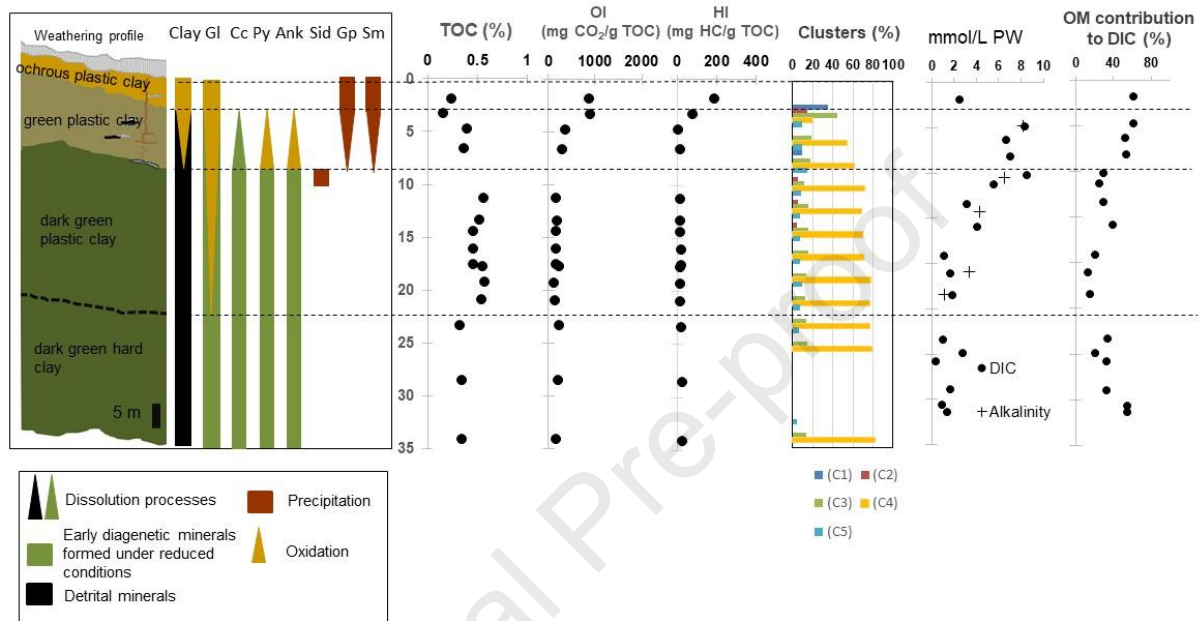
- OM characterization of the Tégulines Clay formation using bulk and molecular data

- Vertical variation of the oxidation profile as a result to the vicinity to the surface

- First upper 10 m of the clays subjected to oxidative events, below 10 m OM preserved

- Spatial variations of the oxidation state due to different topography of the boreholes

- OM bulk and molecular techniques are a good association for critical zone studies

Conflict of Interest

The authors declare that the research was conducted in the absence of any commercial or financial relationships that could be construed as a potential conflict of interest.